Available online at www.jourcc.com

Journal homepage: www.JOURCC.com

Journal of Composites and Compounds

Corrosion behavior of aluminum oxide coatings created by electrolytic plasma method under different potential regimes

*Mahsa Amiri [a], Vahid Tavakoli Targhi [a], Saman Padervand [a], Seyed Mohammad Mousavi khoei [a]**

[a] *Material and Metallurgical Engineering Department, Amirkabir University of Technology, Hafez Street, Tehran, Iran*

ABSTRACT

The electrolytic plasma coating is affected by various factors such as electrolyte conductivity, voltage, and current. However, there has not been much attention to the effect of the current regime. The main objective of the present study is to investigate the potential of Al_2O_3 coatings deposited by the electrolytic plasma method. Aluminum Series 2 was used in this study and the electrolyte was composed of sodium silicate, sodium tetraphosphate, sodium aluminate and potassium hydroxide. The results showed that, in general, according to the impedance diagrams, the corrosion resistance of the coated specimens greatly increases with the immersion time. Therefore, the unit of resistance increased on average to about 10 MHz after 72 hours. In the case of pulsed potential application regime, the corrosion behavior of the samples in the working cycle of 30% was better than that of 70%, which can be related to the thickness of the formed coatings and their porosity. This allows the coating to degrade the coating faster by increasing the thickness and decreasing the porosity of the aggressive chloride ion.

Peer review under responsibility of JCC Research Group

ARTICLE INFORMATION

Article history:
Received 13 June 2020
Received in revised form 27 July 2020
Accepted 19 September 2020

Keywords:
Plasma electrolytic oxidation
Aluminum oxide coatings
Potential regime
Corrosion

1. Introduction

Aluminum and its alloys are of particular importance in the industry due to their light weight, excellent chemical resistance, especially in neutral environments, and high strength to weight ratio [1-3]. They are mainly used in the aerospace, automotive, oil and gas, and drilling industries. Automotive and aircraft parts, pump shells, valves, tanks for transporting petroleum products are among the most important uses of aluminum and its alloys. Aluminum also has many applications in the marine industry. The construction of high-speed vessels is perhaps the most tangible example of this application [4]. Aluminum has good corrosion resistance in many solutions, but in cases where it is in contact with high concentrations of aggressive corrosive agents such as chloride, severe local corrosion occurs [4, 5]. In seawater environment, due to the high concentration of dissolved oxygen, especially chloride ions, the aluminum structures suffer from local corrosion. Therefore, if a suitable surface treatment is performed on aluminum, the service life of aluminum structures and equipment will increase significantly in corrosive environments and it will be used with more confidence [4].

Plasma electrolytic oxidation (PEO) using high voltage is a recently developed surface engineering method [6]. PEO is considered as a method between a common low voltage anodizing in aqueous solutions and a high-energy plasma coating in dry conditions in a controlled gas pressure chamber [7]. PEO can produce ceramic coatings on light metal surfaces with improved properties and the thickness of ten to hundreds of microns [8]. Oxide coatings are produced by high voltage anodic polarization in an electrolyte [9]. Using this method, it is possible to coat aluminum composites as well as hybrid and composite coatings on aluminum substrate [10, 11].

Despite the industrial application of the PEO method, all aspects of this process have not yet been scientifically identified. As a result, PEO is considered as a new method in the field of surface engineering [12, 13]. Despite the excellent mechanical and chemical properties of PEO coatings, researchers are still trying to further improve their properties [14]. It should be noted that parameters affecting the process could severely affect its corrosion and abrasion properties. Among the effective parameters, the type of applied electrical regime can affect the porosity and cracking networks of the coating as well as its chemical composition. Therefore, by selecting the appropriate electrical regime, and controlling the porosity, cracking and the type of formed phases in the coating, better mechanical properties and corrosion resistance can be provided for PEO coatings [12, 15-17].

In order to improve the protective performance of the coating, the defects of the coating must be controlled. Process control can be done with the effective parameters mentioned earlier. Recent research in the field of controlling the structure and morphology of PEO coatings, stress level control and reduction of crack networks are among the most important areas of research in the field of PEO process. In this research, an attempt is made to create enhanced corrosion properties for PEO aluminum coatings by controlling the electrical parameters. Therefore, in this research, aluminum is coated by the PEO process and the effect of

* *Corresponding author: Seyed Mohammad Mousavi khoei; E-mail: Mmousavi@aut.ac.ir*
DOR: 20.1001.1.26765837.2020.2.4.4.6
https://doi.org/10.29252/jcc.2.3.4

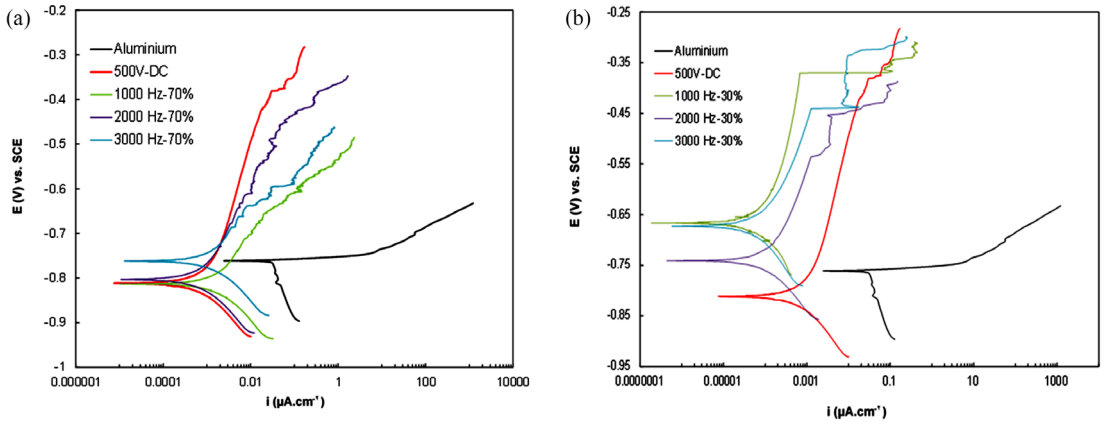

Fig. 1. Polarization diagrams of uncoated aluminum sample and coated aluminum samples with constant potential application of 500 V and application of unilateral pulse potential in different frequencies and operating cycles of (a) 70% and (b) 30% after 72 hours of immersion in 3.5 wt%. sodium chloride solution at room temperature - the solution was static and the potential scan rate was 0.2 mv.sec^{-1}.

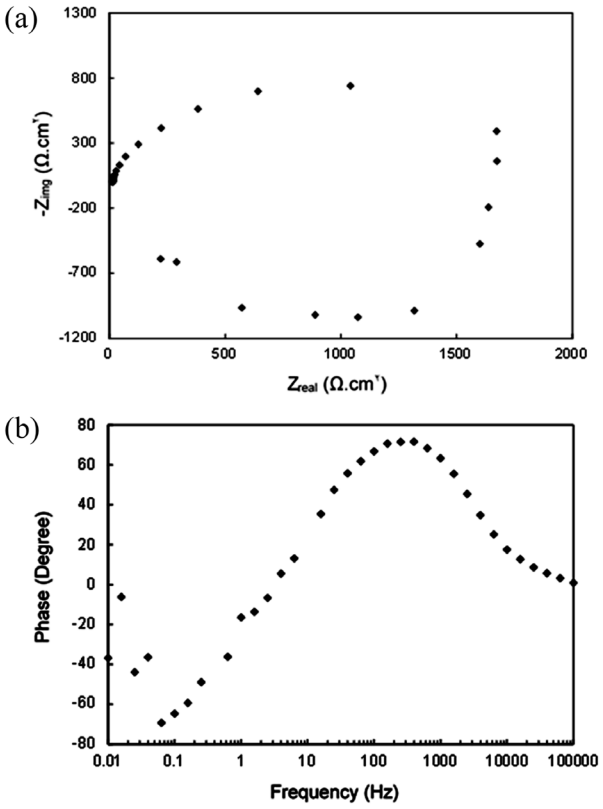

Fig. 2. (a) Nyquist and (b) Bode-phase diagrams of aluminum in 3.5 wt% of sodium chloride at room temperature after 45 min of immersion.

different potential regimes on the corrosion resistance is evaluated.

2. Material and methods

2.1. Materials and sample preparation

In this research, 2025 aluminum sheet with the thickness of 4 mm containing the chemical composition of 0.23% silicon, 0.6% Fe, 0.22% Mg, 0.11% St, 0.03% of Sn (produced by Arak Rolling Company, Iran) was used. Aluminum specimens were cut into 4×20×20 mm dimensions. The surfaces of the samples were sanded by silicon carbide sandpapers up to the grit number of 1800. Then, the samples were cleaned by the ultrasonic method in pure ethanol and distilled water and dried in the air before the PEO process. Based on the initial optimization experiments,

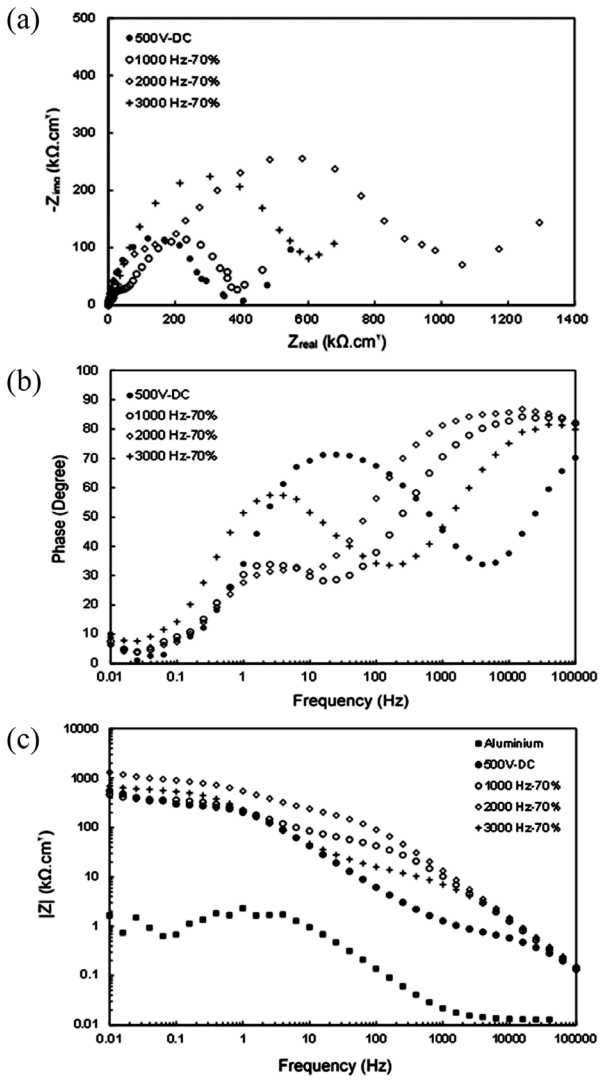

Fig. 3. (a) Nyquist, (b) Bode-phase, and (c) Bode-modulus diagrams of PEO-coated aluminum specimens by applying constant potential and one-way pulse in 70% fixed duty cycle and different frequencies in 3.5 wt% of sodium chloride after 45 min of immersion.

the optimal electrolyte composition of 10 g/l tetra sodium pyrophosphate, 3 g/l sodium aluminate and 3 g/l potash (KOH) was used and according to the obtained morphologies, the coating time of 10 minutes

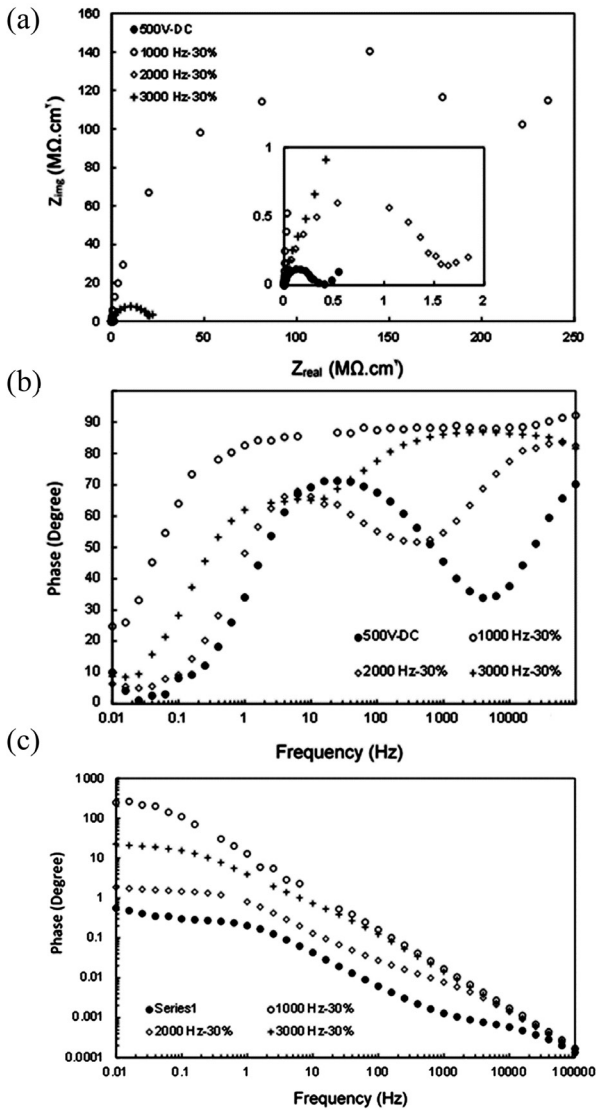

Fig. 4. (a) Nyquist, (b) Bode-phase, and (c) Bode-modulus diagrams of PEO-coated aluminum specimens by applying constant potential and one-way pulse in 30% fixed duty cycle and different frequencies in 3.5 wt% of sodium chloride after 45 min of immersion.

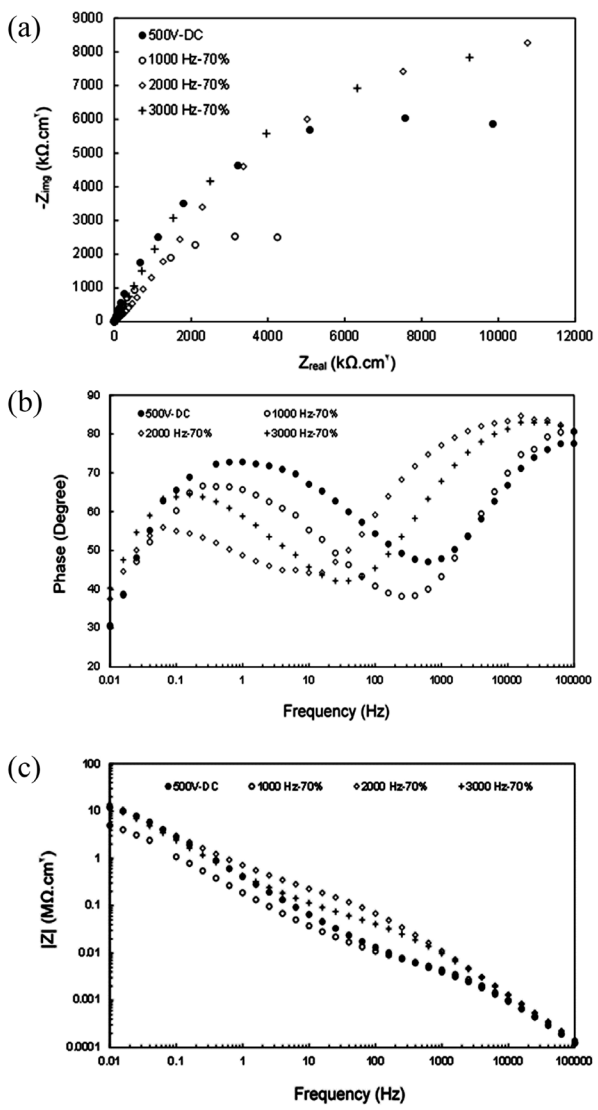

Fig. 5. (a) Nyquist, (b) phase-Bode, and (c) Bode-modulus diagrams of PEO-coated aluminum specimens by applying constant potential and one-way pulse in 70% fixed duty cycle and different frequencies in 3.5 wt% of sodium chloride after 24 h of immersion.

was selected.

2.2. PEO process

The PEO coating was applied on the aluminum surface at a potential of 500 V for 10 minutes. The current density after reaching the potential of 500 V was about 2.5 Am^{-2}. The electric current gradually decreased during the process due to the formation of coating and its thickening.

In the pulse method, the ignition voltage practically occurs earlier than the constant DC mode and due to the high intensity of the generated electric arcs, it is practically impossible to reach the potential of 500 V. Therefore, instead of the potential value, the amount of electric current is considered as a controlling parameter. In other words, when the potential is applied, the potential increases until the current reaches 7 A. Once this current is reached, the potential increase stops and the PEO process continues without the potential increase. Table 1 shows the electrical parameters measured during the PEO process.

Table 1.
The electrical parameters measured during the PEO process. The area of the samples was about 4 cm^2.

Parameter	DC-500V	Duty cycle 70%			Duty cycle 30%		
		1000 Hz	2000 Hz	3000 Hz	1000 Hz	2000 Hz	3000 Hz
Breakdown Voltage (V)	370	341	350	359	263	280	290
Starting Voltage (V)	500	414	438	452	265	291	317
Final Current (A)	1.7	1	1.7	1.6	2.8	1.5	1.9

2.3. Morphological and structural analysis

The phase composition of coatings was evaluated using X-ray diffraction (XRD, Digaku D/max-2500) using Cu Kα radiation at 40 and 100 mA and at 2θ between 20° and 90°. For studying the morphology and thickness of the coating, a scanning electron microscope (SEM) manufactured by Philips XL 30 was used. A 60-EC conductivity meter was used to measure the conductivity of the electrolyte solution. The thickness of the samples was measured using SEM images. Measure-

ments were made at three points of the cross section (maximum, minimum, and the average thickness), and the average of these three values was reported. The thickness measurement was done using a Quanix 7500 thickness gauge.

2.4. Polarization test

Electrochemical polarization tests were performed in a three-electrode cell with EG&G A273A potentiostat/galvanostat. For EIS tests, a Solartron FRA device (SI 1255) coupled with potentiostat/galvanostat was used. The saturated calomel electrode was used as the reference electrode and the graphite rod was used as the auxiliary electrode. Electrochemical impedance tests were performed in the frequency range of 10 mHz-100 kHz with a range of 10 mV (rms) and after reaching the equilibrium potential of the samples. Polarization tests were performed after the immersion period (72 hours) with a scanning velocity of 0.2 mV/s from -150 mV relative to the open circuit potential to about +500 mV relative to the open circuit potential. Electrochemical polarization tests were performed with ACM Gill 8 potentiostat/galvanostat apparatus manufactured by ACM. Polarization diagrams were analyzed to determine TOEFL slopes and corrosion velocities with ACM software (ACM Analysis Version 4). It should be noted that all electrochemical corrosion tests were performed at ambient temperature and in 3.5% (wt%) sodium chloride solution.

2.5. Electrochemical Impedance Spectroscopy (EIS)

In order to create a linear system, the application of alternating voltage of 10 mV was used to disturb the steady state of the system [6]. In this project, Princeton Applied Research Model 1025 made by EG&G Company was used. Saturated calomel reference electrode made by Azar Electrode and the used cell was the same used for the polarization test.

3. Results and discussion

In this study, two polarization and electrochemical impedance tests

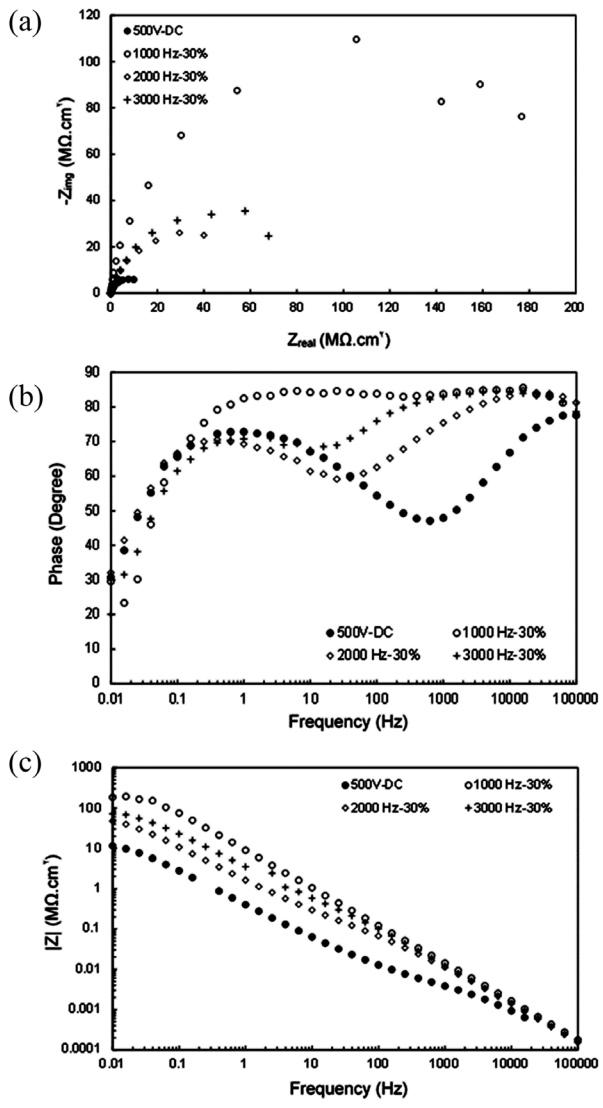

Fig. 6. (a) Nyquist, (b) Bode-phase, and (c) Bode-modulus diagrams of PEO-coated aluminum specimens by applying constant potential and one-way pulse in 30% fixed duty cycle and different frequencies in 3.5 wt% of sodium chloride after 24 h of immersion.

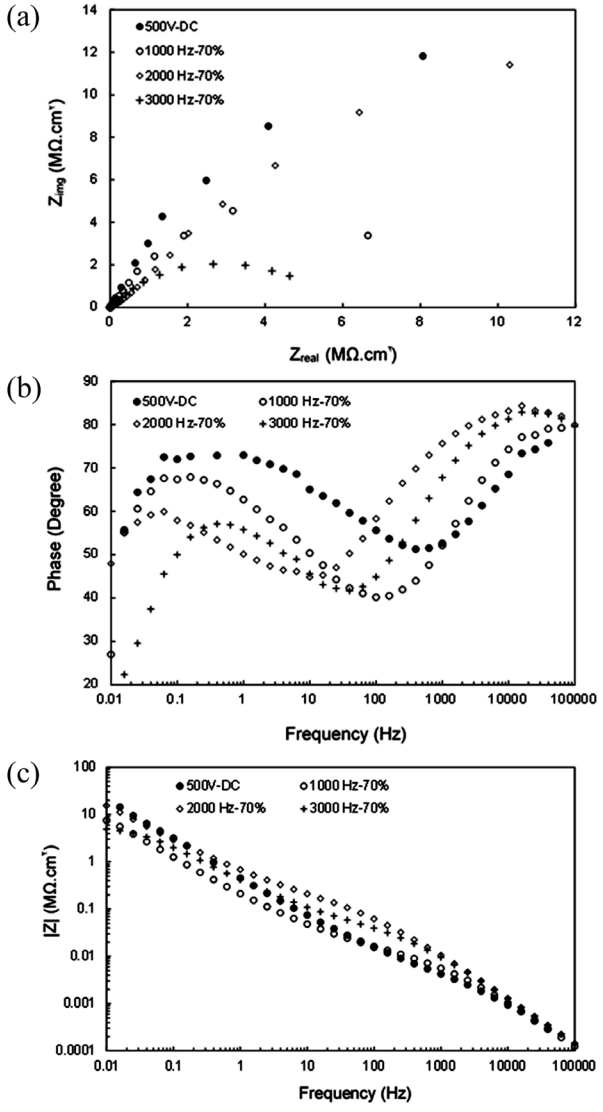

Fig. 7. (a) Nyquist, (b) Bode-phase, and (c) Bode-modulus diagrams of PEO-coated aluminum specimens by applying constant potential and one-way pulse in 70% fixed duty cycle and different frequencies in 3.5 wt% of sodium chloride after 48 h of immersion.

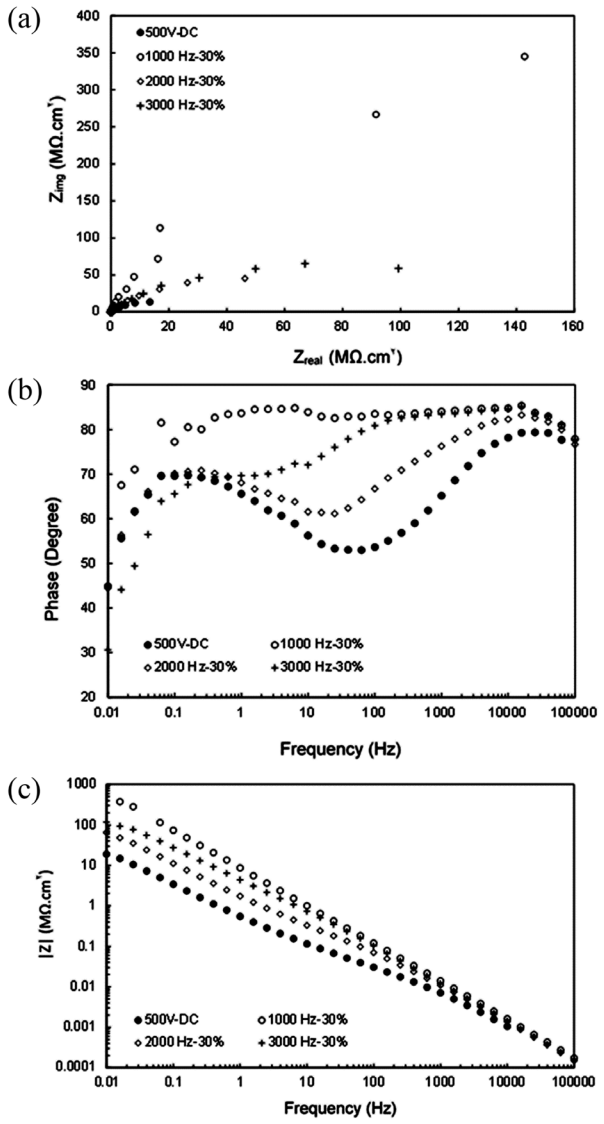

Fig. 8. (a) Nyquist, (b) Bode-phase, and (c) Bode-modulus diagrams of PEO-coated aluminum specimens by applying constant potential and one-way pulse in 30% fixed duty cycle and different frequencies in 3.5 wt% of sodium chloride after 48 h of immersion.

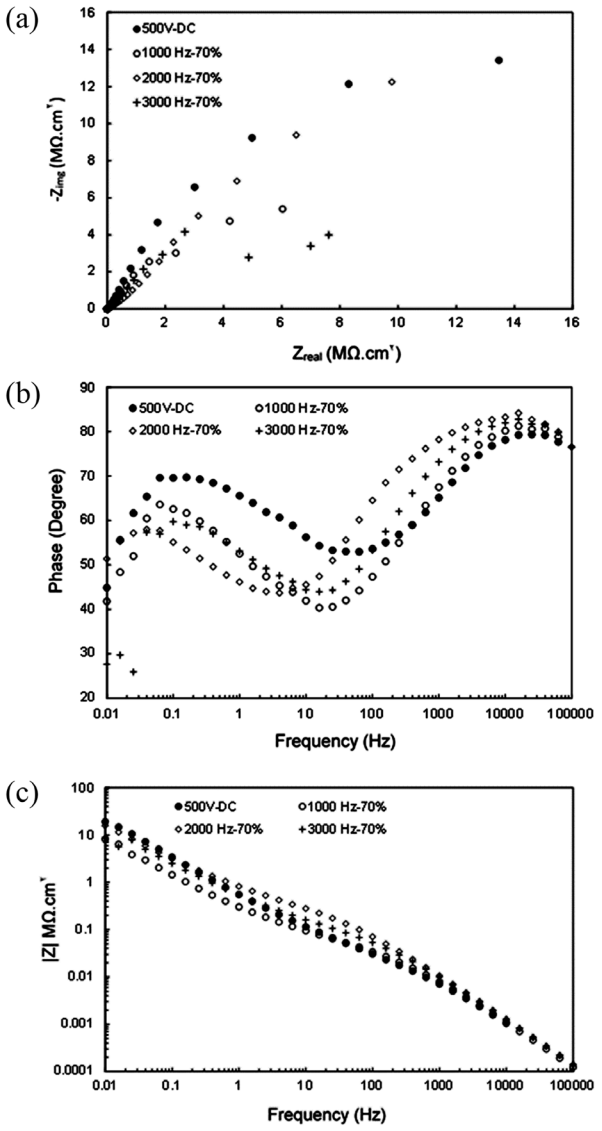

Fig. 9. (a) Nyquist, (b) Bode-phase, and (c) Bode-modulus diagrams of PEO-coated aluminum specimens by applying constant potential and one-way pulse in 70% fixed duty cycle and different frequencies in 3.5 wt% of sodium chloride after 72 h of immersion.

were used to investigate the corrosion resistance and its properties in PEO coatings. Here, the results of these tests will be discussed.

3.1. Polarization test

Fig. 1(a) shows that by creating PEO coatings on the aluminum surface, the polarization diagram is transferred to lower current values. In fact, with the formation of PEO coating, corrosion of aluminum in sodium chloride solution has been reduced by 3.5 wt%. Polarization diagrams have a special behavior in sodium chloride medium. As can be seen, the anode branch of the aluminum polarization diagram experiences a sharp increase in current with a small increase in potential. This type of anodic polarization behavior generally means that the pitting potential is very close to the corrosion potential. In other words, the pitting potential almost overlaps the corrosion potential [18-20]. Under these conditions, the metal or alloy undergoes severe local corrosion in the corrosive environment. Therefore, according to the polarization diagram of uncoated aluminum in Fig. 1(b), it is possible to predict severe local corrosion of aluminum in sodium chloride medium. With the creation of PEO coatings, this behavior is practically not observed and there is almost a considerable difference between the corrosion potential and the pitting potential. Therefore, it seems that the presence of PEO coatings has a positive role in controlling local and pitting corrosion of aluminum. Among PEO coatings, the largest difference between corrosion potential and pitting corrosion potential is observed for the sample coated in the constant potential application regime; in other words, this coating has a better performance than other coatings in preventing local corrosion (pits) on aluminum surface.

The polarization curves of the uncoated and coated samples with a constant potential application of 500 V and a one-way pulse potential application at different frequencies of 70% and 30% duty cycle are shown in Fig. 1. After immersion in 3.5 wt% sodium chloride solution at room temperature, the samples were polarized. As can be seen in the figures, by applying the PEO coating on the samples, polarization curves are shifted to the left and the shift in current density is low, which indicates a decrease in corrosion current in the presence of the PEO coating. Therefore, the PEO coating clearly reduces the corrosion rate of aluminum. Also, according to Fig. 1, the cathodic branches of uncoated and coated samples do not show a significant difference, while in the

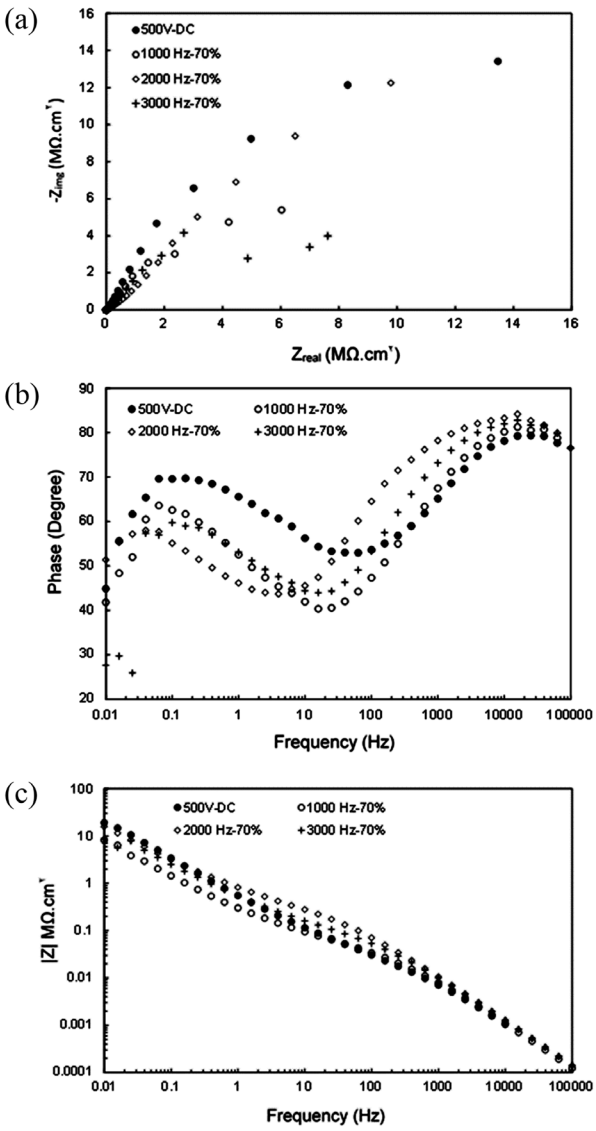

Fig. 10. (a) Nyquist, (b) Bode-phase, and (c) Bode-impedance diagrams of PEO-coated aluminum specimens by applying constant potential and one-way pulse in 30% fixed duty cycle and different frequencies in 3.5 wt% of sodium chloride after 72 h of immersion.

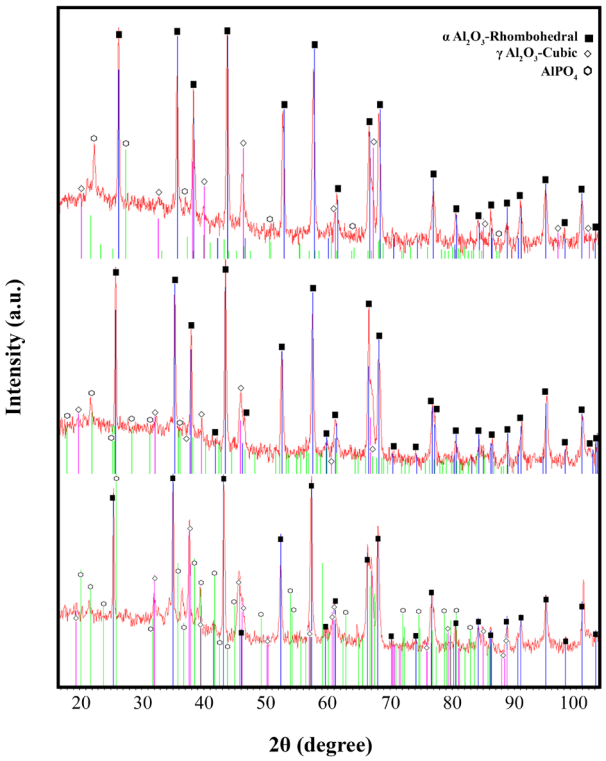

Fig. 11. XRD analysis of phosphorus element in the aluminum sample coated by applying DC-500V potential, one-way pulse potential at 2000 Hz and 70 % work cycles, and one-way pulse potential at 1000 Hz and 30% duty cycle.

Table 3.
Resistance values extracted from impedance diagrams in different immersion times in terms of $cm^2\Omega$

Sample	45 min	24 h	48 h	72 h
Al-bare	200	-	-	-
DC-Coated	4E6	9.8 E3	8E6	13.5E6
1000 Hz-70%	4E6	11 E3	6.6E6	6.3E6
2000 Hz-70%	10E6	4.2 E3	10.3E6	9.7E6
3000 Hz-70%	6E5	9.2 E3	4.6E6	4.8E6
1000 Hz-30%	221.8 E6	176E3	142.8E6	174 E6
2000 Hz-30%	1.6 E6	40E3	46.3E6	46 E6
3000 Hz-30%	22.14E6	67E3	99.3E6	111E6

anodic branches of uncoated samples with a small increase in potential, a sharp increase in current is observed. This means that the corrosion potential (open circuit potential) is very close to the pitting potential of the samples. In other words, by immersing uncoated samples in 3.5 wt.% sodium chloride solution, pitting corrosion occurs, which is practically not observed in the presence of the PEO coating, and there is a significant difference between corrosion potential and pitting potential. As seen, this difference between the pitting potential and the corrosion potential is greater for specimens containing coatings with a duty cycle of 30%, indicating that pitting occurs later in these specimens

Table 1 shows the results of the slope intersection of the anodic and cathodic branches for the polarization curves. As can be seen, data including corrosion current (i_{corr}) and corrosion potential (E_{corr}), slope of anodic and cathodic branches, etc. are obtained from polarization test data. As shown in Table 2, with the application of the coating, the corrosion current decreased significantly from 4.3×10^{-4} to 10^{-5}, indicating a reduction in corrosion in the presence of the coating. Comparing the corrosion current for the coated samples, the coated samples with the duty cycle of 30% shows a greater reduction in the corrosion current, which indicates the suitability of this duty cycle for the improvement of the corrosion resistance.

3.2. EIS test

Fig. 2 shows the Nyquist and Bode diagrams of aluminum in 3.5 wt% sodium chloride medium. As illustrated, the EIS diagrams of aluminum in this solution have a time constant at high and intermediate frequencies and an induction loop at low frequencies. The induction loop with a negative phase angle appears in the Bode-phase diagram (Fig. 2-b). The time constants of the high and middle frequencies are

Table 3.
Parameters obtained from polarization corrosion test

Sample	E_{corr} (mV)	i_{corr} (A.cm^{-2})	β_a (V/decade)	β_c (V/decade)	R_p (Ω.cm^2)	C.R (mm/y)	E_{pitt} (V)	%P
Al-bare	-0.760	3.2E-4	0.013	0.239	16	3.5	~ -0.760	-
DC Coated	-0.812	3.7E-9	0.143	0.090	6562884	4E-5	-0.420	2.7E-10
1000 Hz-70%	-0.814	7.7E-8	0.142	0.093	319865.8	8.35E-4	-0.670	4.11E-9
2000 Hz-70%	-0.803	1.4E-8	0.150	0.093	1718095	62.4E-4	-0.470	5.16E-9
3000 Hz-70%	-0.763	1.6E-7	0.134	0.079	137813.2	671E-4	-0.608	7.85E-5
1000 Hz-30%	-0.667	6.8E-9	0.077	0.062	2175061	7.45E-5	-0.380	7.45E-5
2000 Hz-30%	-0.741	1.1E-9	0.108	0.077	18232089	1.2E-5	-0.465	1.17E-5
3000 Hz-30%	-0.675	1.2E-9	0.137	0.118	23540935	1.3E-5	-0.453	1.28E-5

attributed to the electrochemical interactions of the aluminum surface leading to the formation of the protective layer or surface oxide layer itself. The most common theory for describing this time constant is that it appears due to the corrosion of aluminum at the metal/oxide interface and the formation of Al^+ cations. Due to the presence of a high electric field in the oxide layer, these cations are transferred to the oxide/solution interface, where they are converted to Al^{3+} cations [21, 22].

The reason for the appearance of the induction loop for aluminum in most corrosive environments has not yet been fully identified. Adsorption of intermediate species such as hydroxyl anions, presence of a protective layer on the aluminum surface, rearrangement of surface charges at the metal/oxide interface are the most common theories in this regard [23, 24]. The results of research activities show that the polarization resistance at the emergence of the induction loop (as in Fig. 2) can be estimated by subtracting the diameter of the induction loop from the time constant diameter of high frequencies. Therefore, in Fig. 2, due to the large diameter of the induction loop compared to the time constant of high frequencies, the polarization resistance of aluminum in 3.5 wt.% sodium chloride solution is estimated to be about 200 Ω.cm^2.

Fig. 3 shows the impedance diagrams of aluminum specimens with PEO coating after 45 minutes of immersion in 3.5 wt% sodium chloride solution. As can be seen, the resulting diagrams are different from the aluminum impedance diagrams. In this case, the diagrams have a time constant at high frequencies, a time constant at medium frequencies, and an infiltration sequence at low frequencies. In the Bode diagrams (Fig. 3b and c), two time constants can be seen at high and medium frequencies. According to Nyquist diagrams, the semicircular diameter is the largest for the 2000 Hz specimen and the smallest for DC-500 V.

The observation of the impedance diagrams in Fig. 3 for the samples coated with different potential regimes clearly shows the difference between the different potential regimes. In DC potential mode (500V-DC), the phase angle starts at about 70 degrees and decreases rapidly. With the application of the pulse regime, the initial phase angle is increased to values greater than 80 degrees. In the coating applied at 1000 Hz, the phase angle in the impedance test is maintained up to a frequency of about 2000 Hz in phase angle values greater than 80. By increasing the frequency to 2000 Hz, the time constant of the high frequencies is maintained up to about 500 Hz and then decreases. Generally, in electrochemical impedance tests, the occurrence of high phase angle and its maintenance in a wide frequency range indicates the presence of continuous and dense layers on the metal surface [11, 25, 26]. In the coating applied at 3000 Hz, although the phase angle of time constant of the high frequencies started at about 80 °, it did not behave like the previous two modes (1000 and 2000 Hz). Therefore, according to the results, it seems that the coatings obtained from the pulse regime are denser than the DC coating, and the coating obtained from the pulse regime with a frequency of 2000 Hz at the beginning of the immersion period behaves much better than other coatings.

In the case of Bode module diagrams, the difference in the behavior of the uncoated aluminum sample and the coated samples in different conditions can be easily seen. According to Fig. 3, the overall strength of the aluminum sample is about 21 kΩ.cm, which is about 1000 times for coated samples. The impedance diagrams of the coated specimens under pulsed conditions and a 30% duty cycle are shown in Fig. 4. Among these samples, the frequency of 1000 Hz shows better performance than other samples, and the diameter of the Nyquist diagram of this coating is larger than that of the others. The DC sample has less resistance than the others. In the Bode-phase diagram according to Fig. 4, for a coated sample at a frequency of 1000 Hz over a large frequency range (up to a frequency of 10 Hz), the value of the phase angle is higher than 80. In the 3000 Hz coated sample, the phase angle is higher than 80 up to the frequency of about 300 Hz, but for the 2000 Hz sample and the DC-V500, the phase angle stability is not observed over a wide range. Decreasing and then increasing the phase angle is probably due to the accumulation of corrosion products in the coating pores. Comparing the diagrams of Fig. 3 with Fig. 4, it can be seen that at 24 h immersion time, samples with 70% duty cycle have better corrosion behavior and higher corrosion resistance than 30%.

The impedance diagrams of the samples after 24 hours of immersion are shown in Fig. 5. During this immersion period, the corrosion behavior of all samples is almost the same. Specimens with a frequency of 2000 Hz and 3000 Hz have larger semicircle diameters. In Bode-phase diagrams, the phase angle of all samples at the frequency of 100,000 Hz is almost the same and it suddenly decreases. It seems that during this immersion time, the corrosive solution has entered the coating pores because the phase angle gradually increases with decreasing frequency. The Bode module diagram also clearly shows that the behavior of the coated samples in pulsed mode and at frequencies of 2000 and 3000 is better than other samples.

After a 24 h of immersion, the impedance diagrams for the DC-500 V and pulse samples under the 30% duty cycle are shown in Fig. 6. During this immersion period, the behavior of the coated sample at a frequency of 1000 Hz is shown to be better than other samples. According to the Bode-phase diagram, the phase angle for the sample of 1000 Hz in a wide range of frequency (up to 1 Hz) is higher than 80 degrees. In the case of coated samples at 3000 Hz and 2000 Hz, the phase angle is constant in lower frequency range (approximately up to 900 Hz). In the case of the DC-V500 coated specimen, the phase angle decreases rapidly. This trend can be clearly seen in the Bode-module diagram.

The impedance diagrams during the 48-hour immersion period are shown in Fig. 7. The corrosion behavior of all samples is similar, and the process is similar to that of the 24-hour immersion. During this immersion period, the phase angle decreases immediately. In the Bode-module pattern, the process is similar to the 24-hour immersion time. In the 30% duty cycle, after 48 hours of immersion, the impedance test information is extracted and the results are shown in Fig. 8. The behavior of the samples is similar to that of 24 hours, and for the sample coated at 1000 Hz, the phase angle value is constant over a wide frequency range (approxi-

mately up to 0.5 Hz) and is above 80 °. For the 3000 Hz coated sample, the phase angle is also statically stable and above 80, but for the other 2 samples (the 2000 Hz coated sample and the DC-500 V coated sample), the phase angle suddenly decreases.

After immersion for 72 hours, the results of the impedance test for the DC-500 V potential regime and the pulse potential regime at the frequencies of 1000 Hz, 2000 Hz, and 3000 Hz are plotted as Nyquist and Bode diagrams in Fig. 9. According to the images, the corrosion process has not changed noticeably compared to the previous immersion times. Nevertheless, the corrosion resistance of the coating has increased dramatically. The results of the impedance test after 72 hours of immersion for the DC-500 V sample and pulse samples with a 30% duty cycle are shown in Fig. 10. Similar to the previous immersion time, the coated sample at a frequency of 1000 Hz has the phase angle frequency of about 85 degrees in wider frequency range. According to the Bode-modulus diagram, almost all coated samples show good capacitive behavior in the pulsed mode. In the case of the DC-500V, there is some difference with the capacitive behavior, but in general, the corrosion resistance has increased in all samples.

Generally, according to the impedance diagrams, the corrosion resistance of the coated specimens increases significantly over the immersion time. Therefore, after 72 hours, the resistance increased to an average of about 10 MΩ [27, 28]. Regarding the pulse potential application regime, the corrosion behavior of the samples in the duty cycle of 30% is better than 70%, which can be related to the thickness of the coatings and their porosity percentage [29]. Therefore, by increasing the thickness and decreasing the porosity, the invading chloride ion is able to destroy the coating at a slower rate. The value of resistance, R_p, at different times is summarized in Table 3. In the analysis of the impedance diagrams, other parameters can be also extracted and the corrosion resistance performance of the coating can be examined from other aspects, which will be explained below.

3.3. XRD analysis

To investigate the corrosion behavior, it is better to study the XRD analysis of the coating. For this purpose, the coatings created in the DC potential regime and optimized coatings in terms of corrosion resistance and morphology have been analyzed for further investigation. And the results are shown in Fig. 11. In the PEO coatings, the α phase provides the wear resistance of the coating and the γ phase provides the corrosion resistance. In the XRD images, the coated samples generally show three types of peaks. Fig. 11 shows the sample coated under the DC potential regime under 500 V. It has a lower γ value than the other two samples. This sample has a large amount of α-Al_2O_3 phase and about 30% of it is composed of the γ-Al_2O_3 phase. Also in this composition, some amounts of aluminum phosphate have been observed.

In the samples coated under the pulse voltage regime at the frequency of 2000 Hz and the operating cycle of 70 % (Fig. 11), the amount of aluminum phosphate composition is almost the same as the previous sample. In this sample, α-Al_2O_3 decreases compared to the previous sample and the amount of γ-Al_2O_3 has been increased. In Fig. 11, which is related to the coating at 1000 Hz and 30% duty cycle, the percentage of γ phase reaches about 50%, which is in good agreement with the corrosion diagrams and their corrosion resistance has been increased.

In Fig. 11, there is some aluminum phosphate compound. By increasing the γ phase, the amount of this phase has decreased. It is worth noting that the γ phase is in the form of the tetragonal type. γ-Al_2O_3, regardless of its tetragonal distortions, has always been described as having a cubic spinel structure and a spatial group of Fd3m. Paglia et al. [29] showed that there is also a tetragonal type for γ−Al_2O_3 through neutron diffraction and TEM analysis. In Fig. 11, the XRD result of the 30% sample at 1000Hz is presented, which confirms the presence of this phase with a tetragonal structure in the coating too. One of the interesting points in XRD diagrams is the presence of aluminum phosphate phase in the coating, which may be one of the factors that increase the corrosion resistance of PEO coatings. To confirm the presence of aluminum phosphate phase, the distribution of phosphorus under the substrate was examined.

4. Conclusions

In this research, aluminum was coated by the PEO method in the optimal electrolyte composition of 10 g/l tetra sodium pyrophosphate, 3 g/l sodium aluminate and 3 g/l potash (KOH). The results are summarized as follows:

1. In general, according to the impedance diagrams, the corrosion resistance of the coated specimens increases greatly over the immersion time. After 72 hours, the resistance increased to an average of about 10 MΩ.
2. In the case of pulse potential regime, the corrosion behavior of the samples in the work cycle of 30% is better than 70%, which can be related to the thickness of the coatings created and their porosity.
3. In this way, by increasing the thickness and decreasing the porosity, the invading chloride ion is able to destroy the coating at a slower rate.

Acknowledgments

The authors received no financial support for the research, authorship and/or publication of this article.

Conflict of Interest

All authors declare no conflicts of interest in this paper.

REFERENCES

[1] I. Tajzad, E. Ghasali, Production methods of CNT-reinforced Al matrix composites: a review, Journal of Composites and Compounds 2(1) (2020) 1-9.
[2] K. Zhang, H.W. Jang, Q. Van Le, Production methods of ceramic-reinforced Al-Li matrix composites: A review, Journal of Composites and Compounds 2(3) (2020) 77-84.
[3] F. Sharifianjazi, M. Moradi, A. Abouchenari, A.H. Pakseresht, A. Esmaeilkhanian, M. Shokouhimehr, M.S. Asl, Effects of Sr and Mg dopants on biological and mechanical properties of SiO_2–CaO–P_2O_5 bioactive glass, Ceramics International (2020).
[4] B. Ghorbanian, S.M.M. Khoie, Formation of vanadium carbide with the plasma electrolytic saturation method (PES) and comparison with Thermo Reactive diffusion method (TRD), Acta Metallurgica Slovaca 22(2) (2016) 111-119.
[5] S. Nasibi, K. Alimohammadi, L. Bazli, S. Eskandarinezhad, A. Mohammadi, N. Sheysi, TZNT alloy for surgical implant applications: A systematic review, Journal of Composites and Compounds 2(3) (2020) 62-68.
[6] B. Kasalica, M. Petković-Benazzouz, M. Sarvan, I. Belča, B. Maksimović, B. Misailović, Z. Popović, Mechanisms of plasma electrolytic oxidation of aluminum at the multi-hour timescales, Surface and Coatings Technology (2020) 125681.
[7] T. Kikuchi, T. Taniguchi, R.O. Suzuki, S. Natsui, Fabrication of a plasma electrolytic oxidation/anodic aluminum oxide multi-layer film via one-step anodizing aluminum in ammonium carbonate, Thin Solid Films 697 (2020) 137799.
[8] W. Liu, C. Blawert, M.L. Zheludkevich, Y. Lin, M. Talha, Y. Shi, L. Chen, Effects of graphene nanosheets on the ceramic coatings formed on Ti6Al4V alloy drill pipe by plasma electrolytic oxidation, Journal of Alloys and Compounds 789 (2019) 996-1007.
[9] L. Famiyeh, H. Xiaohu, Improving Corrosion Resistance and Mechanical Properties of Aluminum and its Alloys via Plasma Electrolytic Oxidation (PEO) for Aerospace Applications: A Review.
[10] R. Barik, J. Wharton, R. Wood, K. Stokes, R. Jones, Corrosion, erosion and erosion–corrosion performance of plasma electrolytic oxidation (PEO) deposited Al_2O_3 coatings, Surface and coatings technology 199(2-3) (2005) 158-167.
[11] L. Pezzato, M. Rigon, A. Martucci, K. Brunelli, M. Dabalà, Plasma Electrolyt-

ic Oxidation (PEO) as pre-treatment for sol-gel coating on aluminum and magnesium alloys, Surface and Coatings Technology 366 (2019) 114-123.
[12] V. Dehnavi, B.L. Luan, D.W. Shoesmith, X.Y. Liu, S. Rohani, Effect of duty cycle and applied current frequency on plasma electrolytic oxidation (PEO) coating growth behavior, Surface and Coatings Technology 226 (2013) 100-107.
[13] S.S. Kamble, A. Gunasekaran, S.A. Gawankar, Sustainable Industry 4.0 framework: A systematic literature review identifying the current trends and future perspectives, Process Safety and Environmental Protection 117 (2018) 408-425.
[14] J. Parameswaranpillai, S.K. Sidhardhan, P. Harikrishnan, J. Pionteck, S. Siengchin, A.B. Unni, A. Magueresse, Y. Grohens, N. Hameed, S. Jose, Morphology, thermo-mechanical properties and surface hydrophobicity of nanostructured epoxy thermosets modified with PEO-PPO-PEO triblock copolymer, Polymer Testing 59 (2017) 168-176.
[15] J. Curran, T. Clyne, Thermo-physical properties of plasma electrolytic oxide coatings on aluminium, Surface and Coatings Technology 199(2-3) (2005) 168-176.
[16] V.T. Targhi, H. Omidvar, S.M.M. Hadavi, F. Sharifianjazi, Microstructure and hot corrosion behavior of hot dip siliconized coating on Ni-base superalloy IN-738LC, Materials Research Express 7(5) (2020) 056527
[17] A. Shirani, T. Joy, A. Rogov, M. Lin, A. Yerokhin, J.-E. Mogonye, A. Korenyi-Both, S.M. Aouadi, A.A. Voevodin, D. Berman, PEO-Chameleon as a potential protective coating on cast aluminum alloys for high-temperature applications, Surface and Coatings Technology (2020) 126016.
[18] J. Guest, S. Papavinasam, N.S. Berke, S. Brossia, Corrosion Monitoringand Measurement.
[19] Y. Rao, Q. Wang, D. Oka, C.S. Ramachandran, On the PEO treatment of cold sprayed 7075 aluminum alloy and its effects on mechanical, corrosion and dry sliding wear performances thereof, Surface and Coatings Technology 383 (2020) 125271.
[20] T. Arunnellaiappan, S. Arun, S. Hariprasad, S. Gowtham, B. Ravisankar, N. Rameshbabu, Fabrication of corrosion resistant hydrophobic ceramic nanocomposite coatings on PEO treated AA7075, Ceramics International 44(1) (2018) 874-884.
[21] E. Parfenov, A. Yerokhin, A. Matthews, Impedance spectroscopy characterisation of PEO process and coatings on aluminium, Thin solid films 516(2-4) (2007) 428-432.
[22] A. Bahramian, K. Raeissi, A. Hakimizad, Characterizing of DC-Plasma Electrolytic Oxidation (PEO) Coatings on 7075 Aluminum Alloy.
[23] V.T. Targhi, H. Omidvar, F. Sharifianjazi, A. Pakseresht, Hot Corrosion Behavior of Aluminized and Si-modified Aluminized Coated IN-738LC Produced by a Novel Hot-dip Process, Surfaces and Interfaces (2020) 100599.
[24] E. Akbari, F. Di Franco, P. Ceraolo, K. Raeissi, M. Santamaria, A. Hakimizad, Electrochemically-induced TiO_2 incorporation for enhancing corrosion and tribocorrosion resistance of PEO coating on 7075 Al alloy, Corrosion Science 143 (2018) 314-328.
[25] H.P. Hack, J.R. Scully, Defect area determination of organic coated steels in seawater using the breakpoint frequency method, Journal of the Electrochemical Society 138(1) (1991) 33.
[26] V. Egorkin, S. Gnedenkov, S. Sinebryukhov, I. Vyaliy, A. Gnedenkov, R. Chizhikov, Increasing thickness and protective properties of PEO-coatings on aluminum alloy, Surface and coatings Technology 334 (2018) 29-42.
[27] I.Š. Rončević, Z. Grubač, M. Metikoš-Huković, Electrodeposition of hydroxyapatite coating on AZ91D alloy for biodegradable implant application, Int. J. Electrochem. Sci 9 (2014) 5907-5923.
[28] A. Hakimizad, K. Raeissi, M.A. Golozar, X. Lu, C. Blawert, M.L. Zheludkevich, The effect of pulse waveforms on surface morphology, composition and corrosion behavior of Al_2O_3 and Al_2O_3/TiO_2 nano-composite PEO coatings on 7075 aluminum alloy, Surface and Coatings Technology 324 (2017) 208-221.
[29] G. Paglia, C. Buckley, A. Rohl, B. Hunter, R. Hart, J. Hanna, L. Byrne, Tetragonal structure model for boehmite-derived γ-alumina, Physical Review B 68(14) (2003) 144110.